

Accessing the dynamics of large many-particle systems using Stochastic Series Expansion

Ansgar Dorneich

Institut für Theoretische Physik, Universität Würzburg, Am Hubland, 97074 Würzburg, Germany

Matthias Troyer

Theoretische Physik, ETH Zürich, CH-8093 Zürich, Switzerland

The Stochastic Series Expansion method (SSE) is a Quantum Monte Carlo (QMC) technique working directly in the imaginary time continuum and thus avoiding “Trotter discretization” errors. Using a non-local “operator-loop update” it allows treating large quantum mechanical systems of many thousand sites. In this paper we first give a comprehensive review on SSE and present benchmark calculations of SSE’s scaling behavior with system size and inverse temperature, and compare it to the loop algorithm, whose scaling is known to be one of the best of all QMC methods. Finally we introduce a new and efficient algorithm to measure Green’s functions and thus dynamical properties within SSE.

PACS numbers: 02.70.Ss, 05.10.Ln

I. THE SSE TECHNIQUE

Since their first formulation in the early eighties^{1,2} Quantum Monte Carlo (QMC) methods have become one of the most powerful numerical simulation techniques and tools in many-body physics. The first QMC algorithms were based on a discretization in imaginary time (“Trotter decomposition”) and used purely local update steps to sample the system’s statistically relevant states. These methods require a delicate extrapolation to zero discretization in order to reduce systematic errors. Furthermore, the purely local updates often prove incapable to traverse the accessible states in an efficient way: autocorrelation times grow rapidly with increasing system size.

A more recent class of QMC algorithms, the so-called “loop algorithms”^{5–12}, use non-local cluster or loop update schemes, thus reducing autocorrelation times by several orders of magnitude in some cases. Unfortunately, it is often highly non-trivial to construct a loop algorithm for a new Hamiltonian, and some important interactions cannot be incorporated into the loop scheme. These interactions have to be added as *a posteriori* acceptance probabilities after the construction of the loop, which can seriously decrease overall efficiency of the simulation. Some loop algorithms also suffer from “freezing”^{5,13} when the probability is high that a certain type of cluster occupies almost the whole system.

These insufficiencies can be overcome using the “stochastic series expansion” (SSE) approach together with a loop-type updating scheme (see Ref. 14 and earlier works referenced therein).

- SSE is (almost) as efficient as loop algorithms on large systems.
- It is a numerically exact method without any discretization error.

- It is as easy to construct and general in applicability as world-line methods.

Following Sandvik^{14–16} we briefly outline the basic ideas of SSE now. The central quantity to be sampled in a QMC simulation is the partition function

$$Z = \text{Tr}(e^{-\beta\hat{H}}), \quad (1)$$

where \hat{H} is the system’s Hamiltonian and $\beta = 1/T$ the inverse temperature. Standard QMC techniques¹⁷ split up the exponential into a product of many “imaginary time slices” $e^{-\Delta\tau\hat{H}}$ and truncate the Taylor expansion of this expression after a certain order in $\Delta\tau$, thereby introducing a discretization error of order $\Delta\tau^n$. In SSE, however, one chooses a convenient Hilbert base $\{|\alpha\rangle\}$ (for example the S^z eigenbase $\{|\alpha\rangle\} = \{|S_1^z, S_2^z, \dots, S_N^z\rangle\}$) and expands Z into the power series

$$Z = \sum_{\alpha} \sum_{n=0}^{\infty} \frac{(-\beta)^n}{n!} \langle \alpha | \hat{H}^n | \alpha \rangle. \quad (2)$$

The statistically relevant exponents of this power series are centered around

$$\langle n \rangle \propto N_s \beta, \quad (3)$$

where N_s is the number of sites (or orbitals) in the system. (This follows from Eq. (11) and from $\langle E \rangle \propto N_s$.) We can thus truncate the infinite sum over n at a finite cut-off length $L \propto N_s \beta$ without introducing any systematic error for practical computations. The best value for L can be determined and adjusted during an initial thermalization phase of the QMC simulation: beginning with a relatively small value of L one can start the QMC update process, stop it whenever the cut-off L is exceeded and continue with L increased by 10...20%.

Now let \hat{H} be composed of a certain number of elementary interactions involving one or two sites (such

as on-site potentials, nearest neighbor hopping etc.). In order to obtain a uniform notation we combine those interactions affecting only one site to new “bond” interactions. (One can, for example, take two chemical potential terms $\mu \cdot \hat{n}(\text{site1})$ and $\mu \cdot \hat{n}(\text{site2})$ and form the bond term $\frac{1}{C}\mu(\hat{n}(\text{site1}) + \hat{n}(\text{site2}))$ with the constant C assuring that the sum over all new bond terms equals the sum over all initial on-site terms.) We can thus assume in the following that \hat{H} is a finite sum of “bond” terms \hat{H}_b and that the operator strings \hat{H}^n in (2) can be split into terms of the form

$$\prod_{i=1}^n \hat{H}_{b_i}^{(a_i)}, \quad (4)$$

where b_i labels the bond on which the elementary interaction term operates and a_i the operator type (e.g. density–density interaction or hopping). By introducing “empty” unit operators $\hat{H}^{(0)} = \text{id}$ one can artificially grow all operator strings to length L and obtain¹⁶

$$Z = \sum_{\alpha} \sum_{\{S_L\}} \frac{\beta^n (L-n)!}{L!} \langle \alpha | \prod_{i=0}^L (-\hat{H}_{b_i}^{(a_i)}) | \alpha \rangle. \quad (5)$$

Here $\{S_L\}$ denotes the set of all concatenations of L bond operators $\hat{H}_b^{(a)}$ and n is the number of non-unit operators in S_L .

If we want to sample the (α, S_L) according to their relative weights with a Monte Carlo procedure we have to make sure that the matrix element of each bond operator is zero or negative since in order to fulfill detailed balance we choose the acceptance probability p of a bond interaction to be proportional to its negative matrix element. This requires however that all matrix elements be non-positive. Does a simple redefinition of the zero of energy help? For the diagonal operators we can indeed add the same negative constant C to each of them without changing the system’s properties, and thus make all matrix elements negative or zero. Unfortunately, for the non-diagonal terms an equally simple remedy does not exist. If one can show, however, that such a non-diagonal operator must appear pairwise for the matrix element to be non-zero, its matrix element can be multiplied by -1 without changing the physics of the system. (This corresponds to a gauge transformation on all lattice sites with odd parity.) On non-frustrated lattices this trick is widely applicable, which considerably increases the set of Hamiltonians suitable for SSE. If there are valid world-line configurations carrying an odd number of non-diagonal vertices with positive matrix element – which is typical for Hamiltonians and lattices with frustrations – only the conventional approach of dealing with the sign problem helps^{2–4}: one simulates a new system with the acceptance probability $p' = |p|$ and obtains the estimate of a physical quantity Q in the form

$$\langle Q \rangle = \frac{\langle Q \text{ sign } p \rangle}{\langle \text{sign } p \rangle}.$$

Unfortunately, $\langle \text{sign } p \rangle$ tends to zero exponentially with increasing system size N_s and inverse temperature β , so that the computation time needed to achieve a certain accuracy exponentially increases with $N_s \beta$ and the practically accessible range of system sizes and temperatures is rather limited.

II. LOOP UPDATES

Having outlined the basic idea of SSE we review the non-local updating scheme proposed by Sandvik.¹⁴ In the following figures we illustrate the proceeding by means of a simple physical model: a system of two types of hard-core bosons on a 6-site chain with periodic boundary conditions and Hamiltonian

$$\begin{aligned} H = & -t \sum_{\alpha=1,2} \sum_i \mathcal{P} \left[a_{\alpha,i}^\dagger a_{\alpha,i+1} + H.c. \right] \mathcal{P} \\ & + \sum_{\alpha=1,2} \mu_\alpha \sum_i n_{\alpha,i} \\ & + \sum_{\alpha=1,2} \eta_\alpha \sum_i \mathcal{P} \left[a_{\alpha,i}^\dagger a_{\alpha,i+1}^\dagger + H.c. \right] \mathcal{P} \end{aligned} \quad (6)$$

with

$$\mathcal{P} = \sum_i (1 - n_{1,i} n_{2,i}). \quad (7)$$

The creation operator $a_{\alpha,i}^\dagger$ creates a hardcore boson of type $\alpha = 1$ or 2 on site i . The first term (t) is a nearest neighbor hopping term, the second term (μ_α) the chemical potential and the third term (η_α) pair creation and annihilation. The projection operator \mathcal{P} implements the hard core constraints between the two types of bosons. In the world-line representation – in which the horizontal axis represents the spatial dimension and the vertical axis the propagation level $l = 1 \dots L$ – we symbolize type-1 bosons by single solid lines, type-2 bosons by double lines and empty sites by dotted lines (see Fig. 1).

Sandvik separates the set of all bond operators into three classes: empty operators $\hat{H}^{(0)}$, diagonal operators $\hat{H}^{(d)}$ and non-diagonal operators $\hat{H}^{(nd)}$. The QMC process starts with an arbitrarily chosen initial state $|\alpha\rangle$ and an empty operator string: in Fig. 1, for example, three sites are occupied with type-1 bosons, two sites are empty and on site 2 is occupied by a type-2 particle. Now two different update steps are performed in alternating order: a diagonal update exchanging empty and diagonal bond operators and an operator loop update transforming and exchanging diagonal and non-diagonal operators.

In the diagonal update step the operator string positions $l = 1 \dots L$ are traversed in ascending order. If the current bond operator is a non-diagonal one it is left unchanged; if it is an empty or diagonal operator it is replaced by a diagonal or empty one with a certain probability satisfying detailed balance (i.e. an operator with

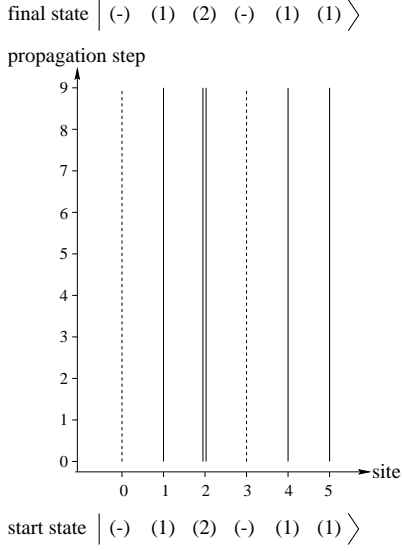


FIG. 1. world-line representation of an arbitrarily chosen start state for a physical system with three allowed occupations per site: empty (dashed line), particle 1 (solid line) or particle 2 (double line). The initial cut-off length L has been set to $L = 9$, and the initial bond operator string consists only of “empty” operators.

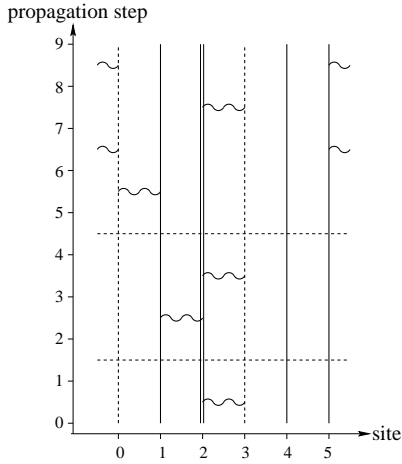


FIG. 2. In the diagonal update step a certain number of empty bond operators is replaced by diagonal ones (and vice versa). In this example seven of the initial nine identity operators have been replaced.

lower energy is more likely to be maintained or inserted than an operator with higher energy) (Fig. 2).

Following Sandvik¹⁴ we use the notation

$$|\alpha(l)\rangle = \prod_{i=1}^l \hat{H}_{b_i}^{(a_i)} |\alpha\rangle \quad (8)$$

for the state obtained by acting on $|\alpha\rangle$ with the first l bond operators and $|\alpha_b(l)\rangle$ for the restriction

of $|\alpha(l)\rangle$ to the bond b . Let M be the total number of interacting bonds on the lattice. Then the detailed balance conditions for the diagonal update read

$$\begin{aligned} P(\hat{H}^{(0)}(l) \rightarrow \hat{H}_b^{(d)}(l)) &= \\ &= \min\left(1, \frac{M\beta\langle\alpha_b(l)|\hat{H}_b^{(d)}|\alpha_b(l)\rangle}{L-n}\right) \\ P(\hat{H}_b^{(d)}(l) \rightarrow \hat{H}^{(0)}(l)) &= \\ &= \min\left(1, \frac{L-n+1}{M\beta\langle\alpha_b(l)|\hat{H}_b^{(d)}|\alpha_b(l)\rangle}\right). \end{aligned} \quad (9)$$

Non-diagonal bond operators cannot simply be inserted into the world line configuration as diagonal operators can: their insertion and modification requires local changes of the world-line occupations. We discussed earlier in this paper that concatenated local changes along a closed path (or loop) through the network of world-lines and interaction vertices are much more efficient than independent purely local changes. Sandvik proposed the following method to construct such a loop: a certain world-line and a propagation level l on it is chosen arbitrarily; at the chosen point one disturbs the world-line by a local change – for example the creation or annihilation of a particle. Then one chooses a direction (up or down in propagation direction) and starts moving the disturbance in this direction (Fig. 3). The aim is to move this disturbance (we will call it “loop head” in the following) through the network of world-lines and interaction vertices until the initial discontinuity is reached again and healed up.

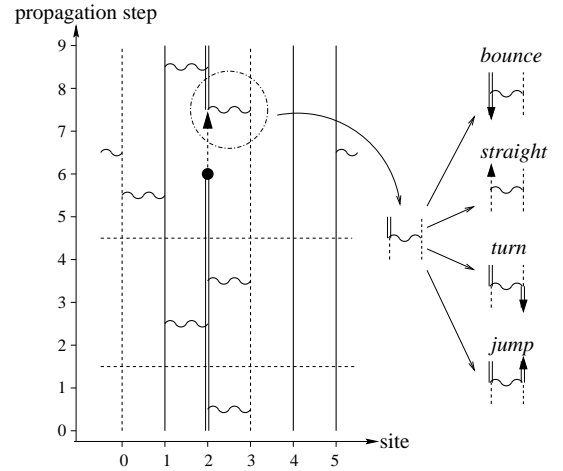


FIG. 3. In the operator loop update step a local change is inserted on a world-line and then moved through the world-lines and vertices. At each vertex a new direction is chosen such that the probability of a path is proportional to the negative energy of the resulting interaction vertex (detailed balance).

Whenever the loop head reaches an interaction vertex we must decide how to go on; in the situation shown in

III. MEASUREMENTS

Efficient estimators for many static observables within the SSE mechanism have been derived by Sandvik.²⁰

- All observables $\hat{H}^{(a)}$ appearing as elementary interactions in the system's Hamiltonian can be measured very easily by counting the corresponding interaction vertices in the bond operator string S_L : if S_L contains on average $\langle N(a) \rangle$ such vertices one obtains

$$\langle \hat{H}^{(a)} \rangle = -\frac{1}{\beta} \langle N(a) \rangle. \quad (10)$$

- Summing over all elementary terms $\hat{H}^{(a)}$ gives an estimator for the internal energy E :

$$E = -\frac{1}{\beta} \langle n \rangle, \quad (11)$$

where n is the number of non-empty interaction vertices in S_L . (This equation can be derived very easily from $\langle E \rangle = \frac{\partial}{\partial \beta} \ln Z$.)

- For the heat capacity C_V we additionally have to measure the fluctuations of n :

$$C_V = \langle n^2 \rangle - \langle n \rangle^2 - \langle n \rangle. \quad (12)$$

- Equal time correlations of two diagonal operators \hat{D}_1 and \hat{D}_2 can be measured via

$$\langle \hat{D}_1 \hat{D}_2 \rangle = \left\langle \frac{1}{n+1} \sum_{l=0}^n d_2[l] d_1[l] \right\rangle, \quad (13)$$

where $d_i[l] = \langle \alpha(l) | \hat{D}_i | \alpha(l) \rangle$.

Are there equally efficient estimators for time-dependent observables? In SSE the propagation index l describes the evolution of an initial state when a series of elementary terms of the Hamiltonian is acting on it; thus l plays a role analogous to imaginary time in a standard path integral. More detailed calculations¹⁵ show that an imaginary time separation τ corresponds to a binomial distribution of propagation distances Δl ; the time-dependent correlation $\langle \hat{D}_2(\tau) \hat{D}_1(0) \rangle$, for example, is related to the correlator

$$C_{12}(\Delta l) = \frac{1}{n+1} \sum_{l=0}^n d_2[l + \Delta l] d_1[l] \quad (14)$$

via

$$\langle \hat{D}_2(\tau) \hat{D}_1(0) \rangle = \left\langle \sum_{\Delta l=0}^n \binom{n}{\Delta l} \left(\frac{\tau}{\beta} \right)^{\Delta l} \left(1 - \frac{\tau}{\beta} \right)^{n-\Delta l} C_{12}(\Delta l) \right\rangle. \quad (15)$$

Instead of working in a representation with varying n a fixed string size L can be chosen, as the identity vertices are uniformly distributed and do not influence the mapping from index to imaginary time.

The corresponding generalized susceptibilities can be calculated straight forward by integrating $\langle \hat{D}_2(\tau) \hat{D}_1(0) \rangle$ over τ ,

$$\chi_{12} = \int_0^\beta \langle \hat{D}_2(\tau) \hat{D}_1(0) \rangle d\tau. \quad (16)$$

which gives¹⁵

$$\chi_{12} = \left\langle \frac{\beta}{n(n+1)} \left(\sum_{l=0}^{n-1} d_2[l] \right) \left(\sum_{l=0}^{n-1} d_1[l] \right) + \frac{\beta}{(n+1)^2} \sum_{l=0}^n d_2[l] d_1[l] \right\rangle. \quad (17)$$

IV. SCALING BEHAVIOR

One decisive criterion for the performance of a QMC simulation technique is the behavior of computation time C as a function of system size N_s or inverse temperature β ; To facilitate a hardware-independent measurement of C and a comparison to other QMC techniques we define C as the number of elementary update operations needed to transform a given state $|\alpha^{(n)}\rangle$ into a new state $|\alpha^{(n+1)}\rangle$ in such a way that the mean autocorrelation time τ is equal to 1. In SSE the number of elementary update operations is the number of diagonal vertices tested for replacement plus the number of vertices traversed during the loop update. In the following we compare SSE to the loop-algorithm, which is known to show an excellent scaling behavior for many benchmark problems. As test models we choose isotropic antiferromagnetic Heisenberg models in one, two and three dimensions with up to 4096 sites and β up to 64 in a vanishing or finite external magnetic field.

Following Ref. 18 we describe the scaling behavior of the two algorithms by means of the dynamical exponent z defined from

$$\tau \cdot C \propto \beta \cdot l^D l^z. \quad (18)$$

Here, $\tau \cdot C$ is the computational effort (i.e. the number of elementary update steps) needed to achieve a mean autocorrelation time of $\tau = 1$ for the measurements of the studied quantity; D is the spatial dimension of the simulated system and $l = \sqrt[3]{N_s}$ its length in each dimension. From Table I we see that both simulation techniques show an approximately equal performance and an very good scaling behavior: since the ratio $C\tau/(\beta N_s)$ is approximately constant we obtain $z \approx 0$ in both cases.

Next we enlarge the square lattice into the third spatial dimension and examine a bilayer quantum Heisenberg

TABLE I. 2D antiferromagnetic Heisenberg model at vanishing magnetic field $h = 0$: calculation of the uniform magnetic susceptibility $\langle \chi \rangle = \frac{\partial \langle M \rangle}{\partial h} \Big|_{h=0}$ from QMC simulations with 1000000 (120000 in the case $\beta = L = 64$) update-measurement cycles (left: SSE, right: loop-algorithm). $C \cdot \tau$ is the number of elementary update operations per cycle needed to achieve a mean autocorrelation time $\tau = 1$ for the measurements of χ .

$\beta \cdot N_s$	SSE		Loop	
	$\frac{C \cdot \tau}{\beta \cdot N_s}$	χ	$\frac{C \cdot \tau}{\beta \cdot N_s}$	χ
$4 \cdot 4^2$	1.00	0.040(46 ± 16)	1.00	0.040(20 ± 10)
$8 \cdot 8^2$	0.61	0.044(83 ± 15)	0.90	0.044(92 ± 8)
$16 \cdot 16^2$	0.40	0.044(72 ± 12)	0.56	0.044(68 ± 6)
$32 \cdot 32^2$	0.40	0.044(19 ± 11)	0.53	0.044(24 ± 6)
$64 \cdot 64^2$	0.36	0.044(01 ± 23)	0.42	0.044(07 ± 14)

TABLE II. Square bilayer antiferromagnetic Heisenberg model at vanishing magnetic field $h = 0$ and at the quantum critical point ($J_{\perp}/J = 2.524$): calculation of the uniform magnetic susceptibility $\langle \chi \rangle$ from QMC simulations with 1000000 (390000 in the case $\beta = L = 32$) update-measurement cycles.

$\beta \cdot N_s$	SSE		Loop	
	$\frac{C \cdot \tau}{\beta \cdot N_s}$	χ	$\frac{C \cdot \tau}{\beta \cdot N_s}$	χ
$4 \cdot 2 \cdot 4^2$	1.00	0.0115(6 ± 7)	1.00	0.0114(6 ± 5)
$8 \cdot 2 \cdot 8^2$	0.96	0.0068(2 ± 6)	1.03	0.0069(2 ± 2)
$16 \cdot 2 \cdot 16^2$	0.68	0.0036(8 ± 4)	1.20	0.0036(6 ± 2)
$32 \cdot 2 \cdot 32^2$	0.56	0.0018(5 ± 3)	1.20	0.0018(3 ± 1)

antiferromagnet at the quantum critical point separating the spin gap phase from the magnetically ordered one.¹⁹ Our aim is to measure scaling behavior and dynamical exponents exactly at this quantum critical point. This point is of particular interest since the immediate neighborhood of a phase transition often leads to the so-called “critical slowing down” of QMC simulations, i.e. exploding autocorrelation times and thus a dramatic decrease of efficiency of the QMC update process.

The results in Table II show that the scaling behavior for both algorithms is still almost linear in βN_s . The scaling for SSE looks slightly superior to the loop algorithm. This difference can most probably be attributed to the fact that improved estimators were used in the loop algorithm simulation, leading to slightly smaller errors but larger autocorrelation times. There is no sign of critical slowing down in either algorithm.

As we have mentioned in the introduction one of the major advantages of SSE is that external potentials (and magnetic fields in spin models) can be included without a loss of performance. To verify this assertion we now ex-

TABLE III. 1D chain antiferromagnetic Heisenberg model in a magnetic field h : calculation of magnetization M from QMC simulations with 1000000 update-measurement cycles (left: SSE, right: loop-algorithm) for a system with $\beta = N_s = 16$. $C \cdot \tau$ is the number of elementary update operations per cycle needed to achieve a mean autocorrelation time $\tau = 1$ for the measurements of M .

h/J	$\beta \cdot h$	SSE		Loop	
		$\frac{C \cdot \tau}{C_0 \cdot \tau_0}$	M	$\frac{C \cdot \tau}{C_0 \cdot \tau_0}$	M
0:02	0.32	1.00	0.008(2 ± 5)	1.00	0.0083(7 ± 7)
0.04	0.64	1.02	0.016(4 ± 6)	0.97	0.017(6 ± 2)
0.1	1.6	1.22	0.057(8 ± 8)	1.84	0.057(7 ± 5)
0.2	3.2	1.98	0.24(4 ± 2)	7.55	0.24(3 ± 2)
0.4	6.4	1.37	0.893(8 ± 9)	167.40	0.89(4 ± 3)
1.0	16.0	0.86	2.069(0 ± 8)	2338.74	2.(24 ± 12)

amine the antiferromagnetic Heisenberg model on a chain and a square lattice in a finite magnetic field $h \neq 0$. For the loop-algorithm we expect to find a rapidly increasing autocorrelation time and decreasing performance if the product of magnetic field h and inverse temperature is much larger than 1. This is due to the fact that the external field is incorporated into the loop-algorithm via a-posteriori acceptance probabilities for each constructed loop. for $\beta h \ll 1$ these probabilities are still large, whereas at $\beta h \approx 1$ they begin to decrease considerably.

Indeed, the numerical results in Table III demonstrate that at $\beta h \approx 10$ the loop algorithm cannot be used any more because the autocorrelation times get too long. For SSE, on the contrary, we do not expect any negative effect by introducing a magnetic field whose strength is of the order of the other elementary interactions, $h \approx J$, since no a-posteriori acceptance decision is necessary. We rather presume that performance is slightly worse for $h/J \ll 1$ because there are elementary interaction vertices with very different energy scales. Both predictions are verified by the data in Table III. For weak fields $h \ll J$ it might be preferable to construct loops in zero field, and to introduce the field via an a-posteriori Metropolis decision on whether to accept loops which change the magnetization, as it is done in the loop algorithm.

For sake of completeness we also show the corresponding data for the 2-dimensional Heisenberg model in Table IV. The results demonstrate that the different behavior of SSE and loop-algorithm described in the one dimensional case is even more severe in two dimensions: the loop-algorithm loses its efficiency already at $\beta h \approx 1.5$.

In some cases other performance measurements are more interesting. One could ask how the computation time till a certain accuracy in a certain measured variable is reached scales with β and N_s . This is studied in Fig. 5. For the square lattice Heisenberg antiferromagnet

TABLE IV. Square lattice antiferromagnetic Heisenberg model in a magnetic field h : calculation of magnetization M from QMC simulations with 1000000 update-measurement cycles for a system with inverse temperature $\beta J = 16$ and $N_s = 16^2$ lattice sites. $C \cdot \tau$ is the number of elementary update operations per cycle needed to achieve a mean auto-correlation time $\tau = 1$ for the measurements of M .

h/J	$\beta \cdot h$	SSE		Loop	
		$\frac{C \cdot \tau}{C_0 \cdot \tau_0}$	M	$\frac{C \cdot \tau}{C_0 \cdot \tau_0}$	M
0:02	0.32	1.00	0.22(4 ± 8)	1.00	0.231(3 ± 3)
0.04	0.64	0.83	0.47(9 ± 8)	1.38	0.477(7 ± 7)
0.1	1.6	0.94	1.41(0 ± 9)	5.61	1.42(2 ± 2)
0.2	3.2	0.44	3.47(0 ± 7)	34.25	3.48(6 ± 7)
0.4	6.4	0.18	7.73(7 ± 4)	1691.66	7.7(8 ± 7)
1.0	16.0	0.12	22.10(6 ± 4)	---	---

we trace the computation time to reach an accuracy of 4 digits in energy as a function of β (Fig. 5 top) and N_s (Fig. 5 bottom). The exponents $\kappa(\beta)$ in $C \propto \beta^{\kappa(\beta)}$ and $\kappa(N_s)$ in $C \propto \beta^{\kappa(N_s)}$ derived from Fig. 5 are

$$\begin{aligned} \kappa(\beta) &= 0.34 \pm 0.05, \\ \kappa(N_s) &= 0.48 \pm 0.05. \end{aligned}$$

Both quantities are smaller than 1, and Eq. (18) would return a negative dynamical exponents z . This is due to self-averaging: in a large system local fluctuations of a physical observable around its mean value on different subregions of the lattice can compensate and average out each other, thereby lowering the observable’s measured variance. The computational effort needed to get thermodynamical averages to a certain relative error scales sublinearly with system size and inverse temperature, so that systems of several thousand sites or at temperatures of not more than $0.001J$ can be simulated within minutes or a few hours on a standard PC or workstation.

V. GREEN’S FUNCTIONS

The observables listed in section III serve to access important static thermodynamic properties of the studied system. However, properties such as photo emission $\langle a^\dagger(\mathbf{k}, \omega) a(0,0) \rangle$ or spin flip $\langle S^-(\mathbf{k}, \omega) S^+(0,0) \rangle$ are often even more interesting as they provide insights into the system’s dynamics. Within the framework of SSE measuring these Green’s functions $G(\mathbf{k}, \omega)$ requires the insertion of local changes on certain world-lines (such as removing a particle at propagation level l_1 on world-line w_1 and re-inserting it at propagation level l_2 on world-line w_2). Performing these insertions is a highly non-trivial task since on the one hand detailed balance must be assured, on the other hand the whole process has to sample all distances $r = w_2 - w_1$ and all propagation

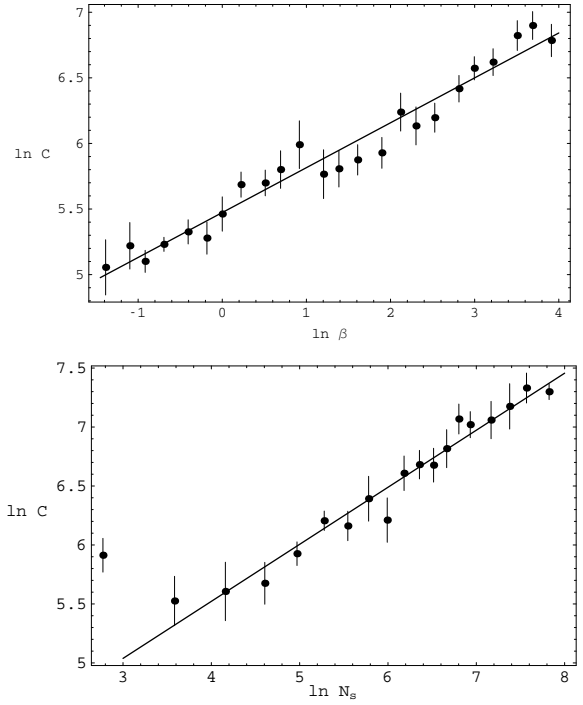


FIG. 5. Scaling behavior of computation time C to reach a relative accuracy of 10^{-4} in the measured energy of the 2D AF Heisenberg model. On top: $\ln(C)$ versus $\ln(\beta J)$ for 10×10 sites. Below: $\ln(C)$ versus $\ln(N_s)$ for $\beta J = 10$. The time was measured in seconds on a DEC workstation.

differences $\Delta l = l_2 - l_1$ efficiently. Both requirements are already fulfilled by the loop update steps. Since this update inserts and moves local changes on the network of world-lines and connecting interaction vertices it can be used to record the corresponding Green’s functions $G(r, \Delta l)$ “on the fly” while constructing the loop update. As an example we reconsider the hard-core boson model from section II and in particular the operator loop shown in Figs. 3 and 4 which starts with the removal of a type-2 particle on propagation level 6 of world-line 2; our cut-off power in the series expansion was $L = 9$, and previous diagonal updates have produced $n = 7$ “non-identity” interaction vertices.

Taking level 6, the starting point of the loop, as zero point for the propagation direction we are now able to measure quantities of type $\langle a_1^\dagger(r, \Delta l) a_2(0,0) \rangle$ and $\langle a_2^\dagger(r, \Delta l) a_2(0,0) \rangle$ during the construction of this loop. Fig. 6 shows that for $\Delta l = 0$ exactly 2 measurements of $\langle a_2^\dagger(r, \Delta l=0) a_2(0,0) \rangle$ and one of $\langle a_1^\dagger(r, \Delta l=0) a_2(0,0) \rangle$ can be performed during the loop: one at the start (or end) of the loop at distance $r = 0$, two on adjacent world-lines ($r = 1$) while moving down (right) and up (left). The recorded value at each measurement is the product of the matrix elements of the creation/annihilation operators inserted at the open ends of the loop under construction. We denote the state at propagation

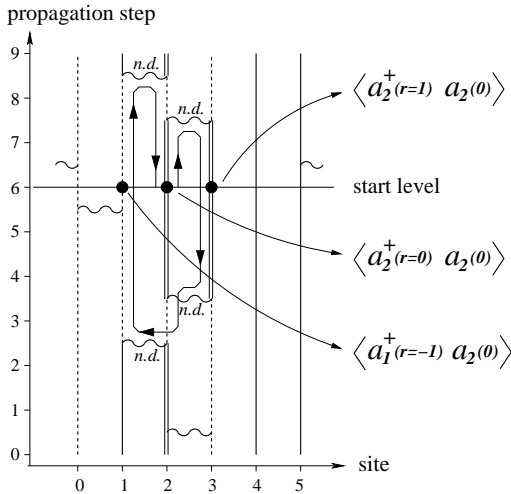


FIG. 6. The loop update constructed in Figs. 3 and 4 can be used to record measurements of the Green's function $\langle a_2^\dagger(r,\Delta l) a_2(0,0) \rangle$ and $\langle a_1^\dagger(r,\Delta l) a_2(0,0) \rangle$ where r is a distance between world-lines (or sites) and Δl is a propagation level difference. For sake of clarity only the measurements for $\Delta l = 0$ are explicitly marked in the figure.

level 6 in our example before inserting the two creation/annihilation operators as $|\alpha(6)\rangle$ and the state after insertion of the operators as $|\tilde{\alpha}(6)\rangle$. Then the $\Delta l = 0$ matrix element $\langle a_2^\dagger(r=1, \Delta l=0) a_2(0,0) \rangle$ – measured when the loop head moves down on world line 3 – is

$$\langle a_2^\dagger(r=1, \Delta l=0) a_2(0,0) \rangle = \langle \tilde{\alpha}(6) | a_2^\dagger(r=1, \Delta l=0) a_2(0,0) | \alpha(6) \rangle.$$

Stepping down by one more propagation level on world line 3 we can record the $\Delta l \neq 0$ matrix element

$$\begin{aligned} \langle a_2^\dagger(r=1, \Delta l=-1) a_2(0,0) \rangle \\ = \langle \tilde{\alpha}(5) | a_2^\dagger(r=1, \Delta l=-1) | \alpha(5) \rangle \langle \tilde{\alpha}(6) | a_2(0,0) | \alpha(6) \rangle. \end{aligned}$$

Leaving our hardcore boson example behind and returning to the general case we conclude this paragraph with the remark that for the creation or annihilation of a fermion the recorded matrix elements are always equal to 1, while they can adopt other values for spin flips or the creation/annihilation of bosons.

Having measured and recorded the quantities $G(r, \Delta l)$ (or a correlation function $C(r, \Delta l) = \langle \hat{D}_2(r, \tau) \hat{D}_1(0, 0) \rangle$) we still have to perform a couple of non-trivial transformation steps till we obtain the desired quantities $G(k, \omega)$ and $C(k, \omega)$ which describe the dynamical response of the system to external perturbations. First we have to relate propagation levels Δl to imaginary times τ , then a Fourier transform brings us from r -space to k -space; finally we need an inverse Laplace transform to step from imaginary time τ to excitation energy ω .

VI. EFFICIENTLY ACCESSING THE SYSTEM'S DYNAMICS

In this section we will discuss efficient implementation strategies for recording $G(r, \Delta l)$ and for the adjacent transformation steps mentioned above.

The transformation from propagation levels Δl to imaginary time τ requires the same weight factors as discussed earlier for diagonal correlation functions:

$$\begin{aligned} G(r, \tau) &= \sum_{\Delta l=0}^n \binom{L}{\Delta l} \left(\frac{\tau}{\beta} \right)^{\Delta l} \left(1 - \frac{\tau}{\beta} \right)^{L-\Delta l} G(r, \Delta l) \quad (19) \\ &\equiv \sum_{\Delta l=0}^L w(\tau, \Delta l) G(r, \Delta l). \end{aligned}$$

where

$$w(\tau, \Delta l) = \binom{L}{\Delta l} \left(\frac{\tau}{\beta} \right)^{\Delta l} \left(1 - \frac{\tau}{\beta} \right)^{L-\Delta l}. \quad (20)$$

Working in a fixed string size representation with fixed L instead of varying n is more convenient because the binomial weight prefactors are fixed during the entire simulation and can easily be calculated once at the beginning of the simulation.

There are several possible ways to implement the recording of $G(r, \Delta l)$ measurements and the adjacent transformation to $G(r, \tau)$. The easiest and at first glance fastest way simply writes all recorded $G(r, \Delta l)$ data into a two-dimensional array with dimensions N_s and $L \propto N_s \beta$. The transformation to $G(r, \tau)$ can then be performed once at the end of the simulation. However, this method has two problems. A separate measurement has to be recorded each time the loop head steps up or down by one level on a world-line and whenever it traverses an interaction vertex. Recording all these measurements drastically slows down the loop update process. Second, for large systems ($N_s \approx 5000$) and low temperatures ($\beta \approx 40$) the two-dimensional array needed to store $G(r, \Delta l)$ contains about 1 billion elements and needs more memory than available on many computer systems.

In order to overcome these problems one can replace the “brute force” recording of data on *all* traversed $(r, \Delta l)$ points by a Monte Carlo sampling: in each loop-update a distance Δl is chosen randomly, according to the probabilities in Eq. (19), for each of the times τ of interest. Measurements are then performed only at these Δl and transformed directly into τ .

In our code we have adopted a third strategy: we perform *all* possible $G(r, \Delta l)$ measurements (thereby exploiting the fact that $G(r, \Delta l)$ is constant on the entire world-line fragment between the adjacent vertices) and directly transform these into $G(r, \tau)$ at the end of each loop update step. The transformation after each QMC update step is necessary to keep memory requirements low.

Simply applying Eq. (19) with its computationally expensive operations (divisions, powers, binomial coefficients, large sums) would now cost by far too much computation time. Instead we remember that $G(r, \Delta l)$ is composed of a relatively small number of intervals $I =]\Delta l_1(I), \Delta l_2(I)]$ with constant function value (Fig. 7b)). Therefore we can compute the contribution of an entire Δl -interval to $G(r, \tau)$ in one step:

$$G(r, \tau) = \sum_I G(r, I) (W(\tau, \Delta l_2(I)) - W(\tau, \Delta l_1(I))), \quad (21)$$

where W is the “integrated weight function”

$$W(\tau, \Delta l) = \sum_{m=0}^{\Delta l} w(\tau, m). \quad (22)$$

The Δl -range in which $W(\tau, \Delta l)$ considerably differs from 0 and 1 is determined by mean value and standard deviation of the binomial distribution $w(\tau, \Delta l)$

$$\langle \Delta l \rangle = L \frac{\tau}{\beta} \quad (23)$$

$$\sigma_{\Delta l} = \sqrt{L \frac{\tau}{\beta} \left(1 - \frac{\tau}{\beta}\right)}. \quad (24)$$

Below $\langle \Delta l \rangle - 5\sigma_{\Delta l}$ the integrated weight is zero, above $\langle \Delta l \rangle + 5\sigma_{\Delta l}$ it is 1 (up to an error of less than 10^{-7}). The remaining interval rarely contains more than fifty or hundred Δl -points (see Fig. 7d); these values can easily be stored after having been computed once for each τ . Thus $W(\tau, \Delta l)$ can be calculated very rapidly with nothing but a couple of “cheap” elementary operations.

For very large systems and very low temperatures the “relevant” Δl -ranges might become so large that it is unfavorable to store all needed $W(\tau, \Delta l)$ values – for example because accessing the large array $W[\tau_i, \Delta l]$ would caust too many cache misses. In this case one can store the coefficients of some interpolation functions for $W(\tau, \Delta l)$ instead of the function values themselves. Practical tests have shown that dividing the relevant interval $[\langle \Delta l \rangle - 5\sigma_{\Delta l}, \langle \Delta l \rangle + 5\sigma_{\Delta l}]$ into six sub-intervals with boundaries $\langle \Delta l \rangle - 5\sigma_{\Delta l}$, $\langle \Delta l \rangle - 2.8\sigma_{\Delta l}$, $\langle \Delta l \rangle - 1.3\sigma_{\Delta l}$, $\langle \Delta l \rangle$, $\langle \Delta l \rangle + 1.3\sigma_{\Delta l}$, $\langle \Delta l \rangle + 2.8\sigma_{\Delta l}$ and $\langle \Delta l \rangle + 5\sigma_{\Delta l}$ and interpolating W in each sub-interval by a fifth-order polynomial is a good compromise between evaluation speed (about 15 elementary operations), storage requirements (36 floating point numbers for each τ) and interpolation accuracy (better than 2.3×10^{-7}).

The next transformation step, Fourier transform from $G(r)$ to $G(k)$, is a well known standard method that does not impose any fundamental problems. However, standard Fast Fourier Transform (FFT) algorithms perform best if *all* $G(k)$ values are to be calculated, whereas in practice one rarely needs all k -values and is interested only in one k -point or in some special points of the Brillouin zone, e.g. the point $k = (\pi, \pi)$ and its immediate

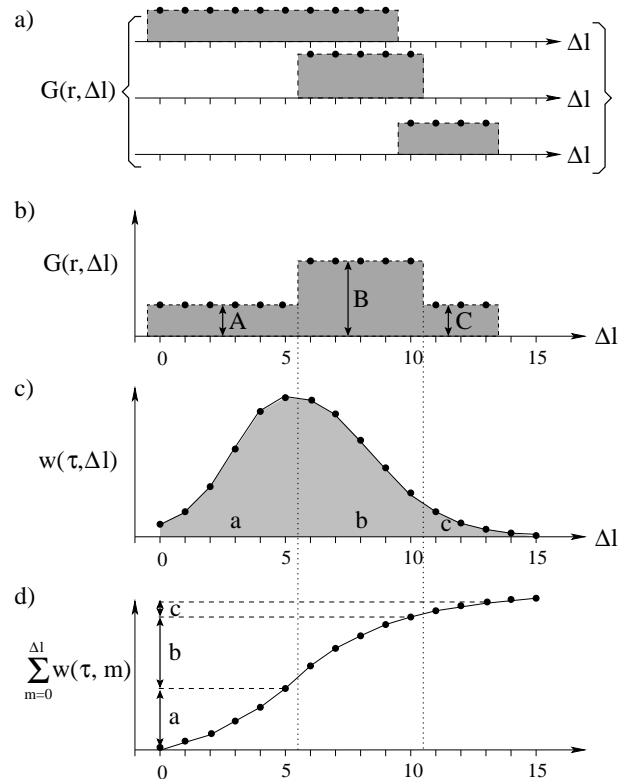


FIG. 7. Transformation of Green’s functions measurements from propagation level Δl to imaginary time τ : the raw measurements recorded during loop update on different world-line segments (a) are combined into a single function $G(r, \Delta l)$ (b). For a given τ $G(r, \tau)$ could be computed by summing up all $G(r, \Delta l)$ weighted with $w(\tau, \Delta l) = \binom{L}{\Delta l} \left(\frac{\tau}{\beta}\right)^{\Delta l} \left(1 - \frac{\tau}{\beta}\right)^{L - \Delta l}$ (c). A much more efficient way uses the “integrated weight function” $W(\tau, \Delta l) = \sum_{m=0}^{\Delta l} w(\tau, m)$ (d) to get the total contribution of each range $]\Delta l_1, \Delta l_2]$ in which $G(r, \Delta l)$ is constant. In the example shown here $G(r, \tau)$ is then simply $aA + bB + cC$.

neighborhood. Then one can save a lot of computation time by not recurring to FFT but using optimized algorithms designed particularly for these cases. If we are interested in only one or a few k -points we can use a simple Fourier transform to get $\{G(k, \tau)\}$ from $\{G(r, \tau)\}$ in $\mathcal{O}(N_s \cdot n_k)$ operations (n_k is the number of k -points). Correlation functions $C(k, \tau)$ can even be measured directly in k -space, which also can be done in $\mathcal{O}(N_s \cdot n_k)$ operations. For the case $1 \ll n_k \ll N_s$ we have implemented a new Fourier transform algorithm performing much better than FFT in this situation.²¹

Unlike a Fourier transform a Laplace transform in general cannot be inverted. Therefore the last transition step from τ to ω is by far more complicated than the previous one from r to k . We use *Maximum Entropy* techniques developed within the last years and refer to earlier publications.²²

VII. EXAMPLE: SPIN CORRELATIONS OF THE 2D HEISENBERG MODEL

In this section we use our standard benchmark model – the saugre lattice Heisenberg antiferromagnet – to test our method of Green’s functions measurements for correctness and numerical efficiency. To this purpose we calculate and compare the correlation functions

$$\langle S^z(\tau, k) S^z(0, k) \rangle \quad \text{and} \quad (25)$$

$$\langle S^+(\tau, k) S^-(0, k) \rangle. \quad (26)$$

In the S^z -eigenbasis, which is normally used to span the model’s Hilbert space, expression (25) is a time-dependent correlation function of two diagonal operators. Therefore the diagonal operator in Eq. (25) can be measured using Eq. (15) without introducing changes in the world-lines and vertices defining the current state of the system. The Green’s function Eq. (26), however, consists of two non-diagonal operators and can only be measured with our new method of recording general Green’s functions that was described in section V. Furthermore, at zero field $h = 0$ both correlation functions are related via

$$\langle S^z(\tau, k) S^z(0, k) \rangle = \frac{1}{2} \langle S^+(\tau, k) S^-(0, k) \rangle, \quad (27)$$

so that the correctness of both estimators can be checked by directly comparing these two quantities.

When working with the antiferromagnet we need to keep in mind that in order to keep the exchange matrix elements S^+S^- and S^-S^+ positive we need to perform a gauge transformation, multiplying S^+ and S^- on one sublattice by -1 . This gauge transformation does not affect any diagonal operator, but leads to a momentum shift of $Q = (\pi, \pi)$, and (27) for the Green’s function and Eq. (27) becomes

$$\langle S^z(\tau, k) S^z(0, k) \rangle = \frac{1}{2} \langle \hat{S}^+(\tau, k + Q) \hat{S}^-(0, k + Q) \rangle. \quad (28)$$

The numerical data in Table V perfectly fulfil this equality and hence demonstrate the correctness of our Green’s functions measurements.

In the simulation recorded in Table V we have calculated $\langle S^z S^z \rangle$ and $\langle S^+ S^- \rangle$ for all allowed k -points on the path $(0, 0) \rightarrow (\pi, 0) \rightarrow (\pi, \pi) \rightarrow (0, 0)$. Table V shows a subset of these points in the vicinity of (π, π) . The three tasks “performing updates”, “measuring $\langle S^z S^z \rangle$ ” and “measuring $\langle S^+ S^- \rangle$ ” contributed the following percentages to overall computation time:

performing updates : 18.8 %
measuring $\langle S^z S^z \rangle$: 36.1 %
measuring $\langle S^+ S^- \rangle$: 45.1 %

From this list and the measurement accuracies in Table V we conclude that the highly non-trivial Green’s functions

TABLE V. Comparison of $\frac{1}{2} \langle \hat{S}^+(k + Q, \tau) \hat{S}^-(k + Q, 0) \rangle$ and $\langle S^z(k, \tau) S^z(k, 0) \rangle$ for the 16×16 -site 2D AF Heisenberg model at $\beta = 16$ and zero magnetic field. The table shows some k -values around (π, π) .

k	τ	$\langle S^z(k, \tau) S^z(k, 0) \rangle$	$\frac{1}{2} \langle S^+(k+Q, \tau) S^-(k+Q, 0) \rangle$
$(\frac{\pi}{2}, \frac{\pi}{2})$	0	0.16(89 ± 20)	0.168(2 ± 4)
	0.1	0.00(01 ± 17)	0.003(2 ± 3)
	0.5	-0.00(36 ± 15)	-0.000(4 ± 3)
$(\frac{3\pi}{4}, \frac{3\pi}{4})$	0	0.38(39 ± 21)	0.386(0 ± 6)
	0.1	0.01(74 ± 20)	0.020(9 ± 5)
	0.5	0.00(41 ± 19)	0.000(4 ± 4)
(π, π)	0	11.3(35 ± 17)	11.36(1 ± 9)
	0.1	10.4(04 ± 17)	10.42(3 ± 9)
	0.5	9.0(83 ± 17)	9.09(3 ± 9)
$(\frac{3\pi}{4}, \pi)$	0	0.53(85 ± 23)	0.542(2 ± 7)
	0.1	0.06(31 ± 20)	0.063(0 ± 6)
	0.5	0.00(38 ± 17)	0.000(0 ± 5)
$(\frac{\pi}{2}, \pi)$	0	0.28(92 ± 23)	0.287(6 ± 5)
	0.1	0.01(08 ± 19)	0.008(5 ± 4)
	0.5	0.00(06 ± 17)	0.000(3 ± 4)

measurements lead to a slightly better accuracy than the direct $\langle S^z(\mathbf{r}, \tau) S^z(\mathbf{r}', \tau') \rangle$ measurements while consuming roughly the same amount of computer time as the latter. Measuring the Green’s function is thus the preferred method of determining also the diagonal real space dynamical correlation functions.

VIII. SUMMARY

Stochastic Series Expansion (SSE) together with the implementation tricks and Green’s functions measurements described in this paper is a highly performant quantum Monte Carlo simulation technique allowing to access both static and dynamical properties of very large systems of thousands of sites and at very low temperatures. Compared to the loop-algorithm, which is slightly faster on big systems for some specific Hamiltonians, SSE has the advantages of not suffering from exponential slowing down in external fields; furthermore, SSE is more easily applicable to wide classes of Hamiltonians.

We thank A. Sandvik for valuable discussions. This work was supported by DFG HA 1537/16-1,2 and KONWIHR OOPCV (A. D.) and the Swiss National Science Foundation (M. T.). High performance calculations were performed at HLRZ Jülich and LRZ Munich.

- ¹ M. Suzuki, Prog. Theor. Phys. **65**, 1454 (1976).
- ² J. E. Hirsch, R. L. Sugar, D. J. Scalapino and R. Blankenbecler, Phys. Rev. B **26**, 5033 (1982).
- ³ M. Takasu, S. Miyashita and M. Suzuki, Prog. Theor. Phys. **75**, 1254 (1986).
- ⁴ N. Hatano, J. Phys. Soc. Japan **63**, 1691 (1993).
- ⁵ H. G. Evertz, G. Lana and M. Marcu, Phys. Rev. Lett. **70**, 875 (1993).
- ⁶ H.G. Evertz and M. Marcu, in *Lattice 92*, Amsterdam 1992, ed. J. Smit et al., Nucl. Phys. B (Proc. Suppl.) **30** (1993) 277, and in "Quantum Monte Carlo Methods in Condensed Matter Physics", ed. M. Suzuki, World Scientific 1994, p. 65.
- ⁷ U.-J. Wiese and H.-P. Ying, Phys. Lett. A**168**, 143 (1992); Z. Phys. B**93** (1994) 147.
- ⁸ N. Kawashima, J.E. Gubernatis, and H.G. Evertz, Phys. Rev. B**50** 136 (1994).
- ⁹ N. Kawashima and J.E. Gubernatis, Phys. Rev. Lett. **73**, 1295 (1994).
- ¹⁰ N. Kawashima, J. Stat. Phys. **82**, 131 (1996).
- ¹¹ N. Kawashima and J.E. Gubernatis, J. Stat. Phys. **80**, 169 (1995).
- ¹² H.G. Evertz, in "Numerical Methods for Lattice Quantum Many-Body Problems", ed. D.J. Scalapino, Addison Wesley Longman, Frontiers in Physics (1998).
- ¹³ M. Kohno and M. Takahashi, Phys. Rev. B **56**, 3212 (1997).
- ¹⁴ A. W. Sandvik, Phys. Rev. B **59**, R14157 (1999).
- ¹⁵ A. W. Sandvik and J. Kurkijärvi, Phys. Rev. B **43**, 5950 (1991); A. W. Sandvik, J. Phys. A **25**, 3667 (1992).
- ¹⁶ A. W. Sandvik, Phys. Rev. B **56**, 11678 (1997).
- ¹⁷ W. von der Linden, Phys. Rep. **220**, 53 (1992).
- ¹⁸ B. Li, N. Madras and A. D. Sokal, J. Statist. Phys. **80**, 661-754 (1995).
- ¹⁹ A. W. Sandvik and D.J. Scalapino, Phys. Rev. Lett. **72**, 2777 (1994).
- ²⁰ A. W. Sandvik, R. R. P. Singh and D. K. Campbell, Phys. Rev. B **56**, 14510 (1997).
- ²¹ A detailed description of the new method will soon be submitted to Comp. Phys. Comm., and a C++ code package will be available from the CPC program library.
- ²² W. von der Linden, R. Preuss and W. Hanke, J. Phys.: Condens. Matter **8**, 3881 (1996).